Mustansiriyah Journal of Pure and Applied Sciences, Print ISSN: 2957-9910. Online ISSN: 2957-9929, Vol. 4, No. 3, 2026, Pages 72-79
DOI: 10.47831/mjpas.v4i3.442

MJPAS

MUSTANSIRIYAH JOURNAL OF PURE AND APPLIED SCIENCES

Journal homepage:
https://mjpas.uomustansiriyah.edu.iq/index.php/mjpas

RESEARCH ARTICLE - PHYSICS

Double Core PCF Sensor with Au-HfO$_2$ Hybrid layer Based on SPR

[1] Muna M. Jassem, [2] Adnan H. Mohammed
[1] Department of Chemestry, Science College, Mustansiriyah University, Baghdad, Iraq.
[2] Department of Physics, College of Education, Mustansiriyah University, Baghdad-Iraq
* Corresponding author Email: Mona.M.Jassim@uomustansiriyah.edu.iq

Article Info.

Article history:

Received
2 June 2025

Accepted
26 August 2025

Publishing
30 September 2026

Abstract

Double core photonic sensor design based on surface plasmon resonance (SPR) that is the base of A photonic crystal fiber (PCF) sensor is designed with a hexagonal structure It uses a hybrid material design integrating gold (Au) and Hafnia (HfO$_{2)}$ layers. The latter is considered as active plasmonic material at which SPR is rapidly excited. Software called COMSOL Multiphysics is used to design and data analysis for suggested sensor. Finite element method (FEM) that is a full-wave numerical technique is carried out to obtain the approximate solutions for electromagnetic boundary value problems The proposed sensor has a detection range of refractive index (RIs) from 1.38 to 1.42 which optimized in spectrum range from 0.5 to 1.2μm . The sensitivity (S_λ) has a large value at RI of 1.41 to be 39310 (nm/RIU) that associated with the highest sensor resolution of 2.54×10^{-7} RIU . The resonance wavelength peak (λ_P) and peak loss exhibit are increased nonlinearly while of FWHM, the findings show that the non-linearity tendency is dominant; it increases rapidly with RIs of analyte. lastly, figure of merit (FOM) has larger value at maximum S_λ where the highest values of FOM attains maximum values of S_λ. The maximum S_λ attained at RI difference 1.41 and 1.42 makes the proposed sensor has the capability to detect minor RIs difference of 0.001. Use the distinct optical characteristics of Au and HfO$_2$, the sensor has achieved confinement and exhibits excellent performance metrics.as presented in the paper.

The official journal published by the College of Education at Mustansiriyah University

Keyword: ***PCF*, hybrid photonic materials, *SPR* sensor, *HfAu − PCF* sensor.**

1. Introduction

Sensors made with optical fibre have transformed the sensing domain by providing several benefits, including exceptional sensitivity, small dimensions, and capabilities for remote sensing [1]. PCF sensors are distinguished from other types of optical fibre sensors by its distinct design adaptability and exceptional optical properties [2, 3]. These optical fibre sensors provide exceptionally sensitive and accurate measurements across several applications, including medical diagnostics and environmental monitoring [5 ,4] . Although conventional fibre optic sensors provide satisfactory performance, the pursuit of enhanced researchers are exploring new directions in material science and fibre geometry as a result of sensitivity and resolution [6, 7]. Most contemporary research is on plasmonic photonic crystal fibre sensors using metals such as gold ,silver, or carbon-based material, like the graphene [8, 9]. Nonetheless, these materials frequently possess inherent restrictions, such vulnerability to oxidation, elevated prices, or intricate production processes [10, 11]. Recent studies have begun investigations into innovative materials such as graphene, HfO$_2$, and Au, recognized for their distinctive optical characteristics and compatibility [12-14]. Au layer-based SPR sensor demonstrates encouraging results regarding adaptability and sensitivity [15, 16]. Innovative material are investigated to developed a variety of sensors of SPR, including as biosensors, temperatures sensor, and SPR resonance-based refractive sensors [17]. Materials including a mixture of HfO2 and an layer of Au warrant consideration because to HfO$_2$ elevated refractive index, little attenuation, with the superior optical characteristics of gold [18]. In this work, we seek to address this deficiency by presenting a new HfO$_2$-Au Photonics Crystals Sensors that utilizes design of hybrid material integrating HfO$_2$ and a layer of Au. The architecture presented in [19]. has been updated to incorporate a nanolayer HfO$_2$ and Au, as well as, a central hole. The adjustment has achieved significant results where the findings show that the maximum S_λ is 39310 nm/RIU associated with resolution 2.54×10^{-7} RIU within the spectrum range

500 to 1100nm. These results are larger than the listed [20] that are 10800 nm/RIU and 28700 nm/RIU for RIs from 1.41 to 1.42 and 1.42 to1.43, respectively. The compared values were for structure like proposed in the paper without using HfO_2 layer. The use of HfO_2 attained maximum S_λ for RIs (1.41 and 1.42) and this makes there is a capability for detecting minor RIs differences of 0 .001.

2. Structure designing and numerical implementation

Generation of SPR phenomena in a PCF depends on the intensity of incoming evanescent electromagnetic (EM) fields and the oscillation of the surface of free electron density. The diffusions of the Evanescence's waves in the clad of PCF arise when electromagnetic fields propagate in the core region. SPW is created when the resonance condition has satisfied, that is, in the case of equality for n real part for both core guided and SPPs modes. SPW at resonance wavelength is maximum value has a prominent peak in the loss spectra of the core mode. As a consequence, the tiny variations will cause the shifting of resonance wavelength [21]. Thickness of Au and HfO_2 layer is 0.02 μm while of analyte and PML, respectively, are 0.75 μm and 0.8 μm. The lattice constant in y-direction is equal to 0.86 μm of pitch in x-direction and its value is 1.5 μm. The design of a typical sensor system configuration with non-real scale is shown in Fig. 1(a) which explains a visual depiction of a suggested SPR based on a twin core PCF sensor with a central hole and a diameter of the first inner circle was 7.42 μm. The cladding holes diameter is 1μm that optimized to be the results as will exhibit in this paper. The diameter of the center hole is 0.8 μm while equal two holes up and bottom of central hole is1.2 μm. A diameter of two holes at the horizontal line which passes the central hole is 0.4 μm. Fig. 1(b) explains the experimental set up for proposed sensor.

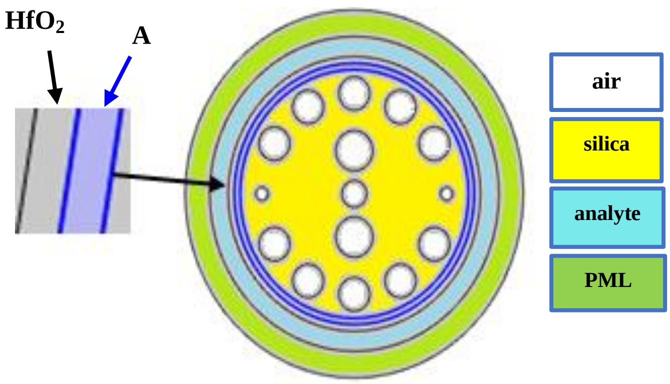

Fig. 1: (a) The cross section of suggested model structure.

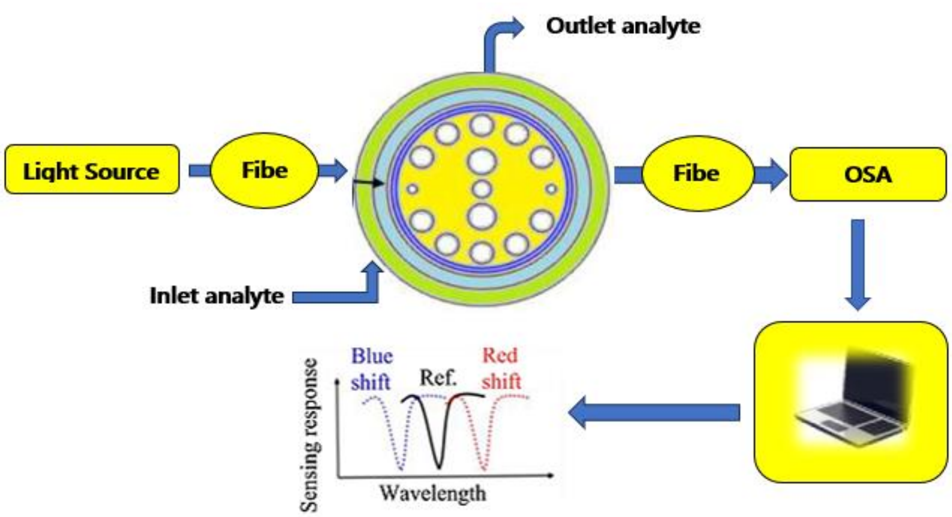

Fig. 1: (b) Determination the sensor function and position within the experimental setup.

3. Description of used material

The even, odd modes of (x-y) polarization are simultaneously activated when energy enters the dual-core PCF − SPR biosensor’s that is part of the proposed sensor. In our work, even x-polarized mode has a larger mode losses’ and can betters coupled with the medium of metal medium sensor, so, we focus for mentioned polarization type. The solid black line and blue line in the Fig. 2 show a real part of the SPP and FM modes, respectively, while red color present resonance wavelength.

The SPR − PCF biosensor's geometrical design structure is completed, and COMSOL Multiphysics 6.1 software is used to assess the biosensor's properties. To give mathematical description of the proposed geometrical design then the following equations inside COMSOL software environment that express the relation between RI and wavelength can be determined. Firstly, the background material of proposed sensor is silica and its dependence on the wavelength can be expressed by [22].

$$n(\lambda) = \sqrt{1 + \sum_{i=1}^{3} \frac{B_i^3}{\lambda^2 - C_i^3}} \quad (1)$$

$B1 = 0.691663,\ B2 = 0.407943,\ B3 = 0.897479400, C1 = 0.004679\ \mu m^2,\ C2 = 0.013512\ \mu m^2$ and $C3 = 97.934003 \mu m^2$. λ wavelength of incident light. To express dielectric function of gold as plasma material, one can use the Drude-Lorentz model (DLM). It is complex dielectric function $\epsilon_r(w)$ which may be expressed as [23].

$$\epsilon_r(w) = w_r^f(w) + w_r^b(w) \quad (2)$$

It specifically distinguishes between intraband effects (typically known as free-electron effects) and interband effects (generally known as bound-electron effects). DLM is a complex dielectric permittivity with a Drude component for the intraband effect (first term) and a Lorentz component for the interband transition impact (second term). [24].

$$\epsilon_r(w) = 1 - \frac{\Omega_p^2}{w(w - i\Gamma_o)} + \sum_j^k \frac{f_i\, w_p^2}{(w_j^2 - w^2 - iw\Gamma_j} \quad (3)$$

Here, w_p denotes the plasma frequencies, k represents the quantity of oscillator characterized by frequency w_j, strength f_i, and duration Γ_j j. Additionally, $\Omega_p = (f_o)^{0.5} w_p$ signifies the plasma frequency linked to intraband transitions, characterised by oscillator strength f_o and damping constant Γ_o. In noble metals, several interband transitions may occur owing to the diverse band structures of bound electrons. The specified metals has predominantly utilized in opto − electronic device’s. Optical measurements are significantly influenced by experimental variables, including geometry, morphology, and manufacturing processes; hence, the relevant optical data must be meticulously selected. The refractive index of Au according to LDM and by using the coefficients in Table 1 will be complex while the dispersion relation of HfO_2 is given by [25].

$$n(\lambda) = 1.875 + \frac{6.28 * 10^{-3}}{\lambda^2} + \frac{5.80 * 10^{-4}}{\lambda^4} \quad (4)$$

Table 1. Parameters of the LD Model Values

Parameter	Value	Parameter	Value	Parameter	Value
f_o	0.760	Γ_2	0.345	Γ_4	2.494
Γ_o	0.053	w_2	0.830	w_4	4.304
f_1	0.024	f_3	0.071	f_5	4.384
Γ_1(eV)	0.241	Γ_3	0.870	Γ_5	2.214
w_1(eV)	0.415	w_3	2.969	w_5	13.32
f_2	0.010	f_4	0.601		

RI of Au according to LDM will be (real and image. part) and HfO_2 versus λ can be plotted in MATLAB environment as shown in Fig 2 to obtain one of Au and other for HfO_2. After that, the description of Au and HfO_2 inside COMSOL

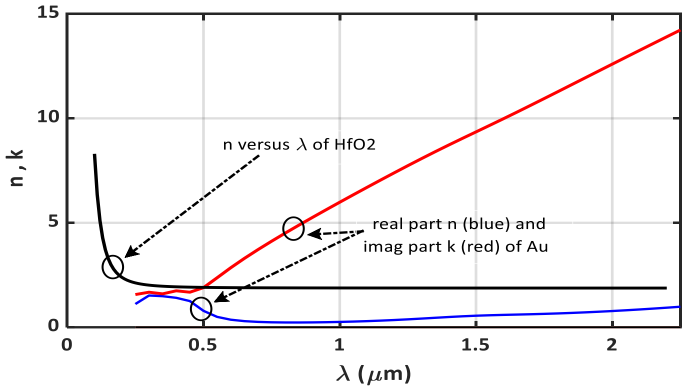

Fig. 2. RI of HfO_2 and gold (real and imaginary part) versus wavelength.

environment become perfect. The dispersion relation used in representation fig. 4 determined into Eqs. 4 and 5. For remaining material such as air holes, RI is considered to be 1 and mentioned a above is intended to be closest to the surface layer for absorbing light dispersed from PCF surface throughout the simulation [19].

4. Result and discussion

Fig. 3 shows the phase match procedure transpires at a wavelength of 650 nm and the peak loss is 42.9 dB/cm , the latter occurs at this wavelength for analytes with a RI of 1.41. Also, the same figure shows the maximum energy is transfer from the FM mode to SPP mode transpires at that wavelength, resulting in resonance and the generation of surface plasmons. The losse's in a plasmonic layer are quantified in dB/cm using the following recipe [26].

$$\alpha_{loss} = 8.686 \times k_o \times \mathrm{Im}(n_{eff}) \times 10^4 \qquad (5)$$

where $\mathrm{Im}(n_{eff})$ denotes an imaginary part of a refractive index and $k_o = 2\pi/\lambda$ refers to number of wave whereas the value of will be λ is in micrometer.

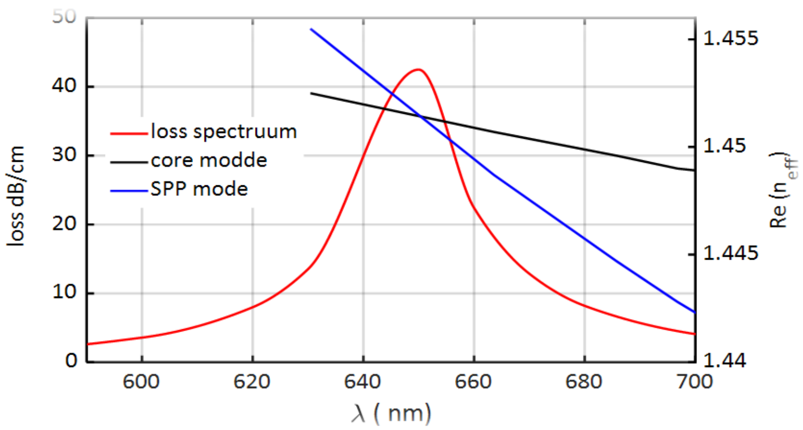

Fig 3. The SPR biosensor's confinement loss, core and SPP mode dispersion relations RI = 1.41.

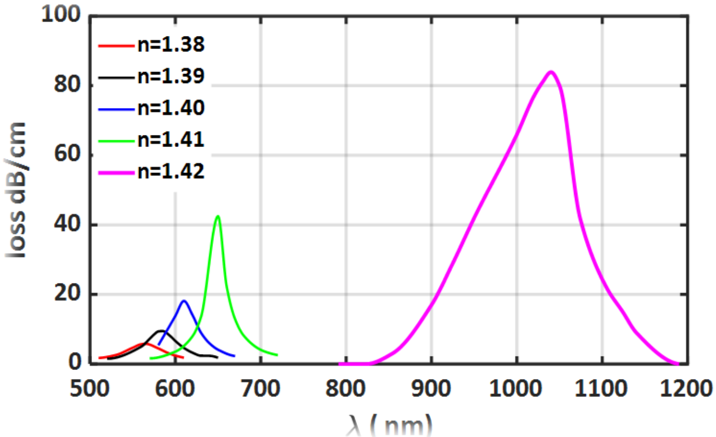

Fig. 4. Loss septum for different RIs of analytes.

Fig**. 4 shows** the loss with changing analyte RI from 1.38 to 1.42 with step increasing of 0.01. To evaluate the performance of an SPR sensor, the loss peak is well known and suitable to do that. As a consequence, the sensitivity that calculated by the following equation [27]. Will be improved with RI increase

$$S_\lambda(nm/RIU) = \frac{\Delta\lambda_{peak}}{\Delta n_{anal.}} \quad (6)$$

$\Delta\lambda_{peak}$ is the difference of resonance wavelength for successive refractive index ($\Delta n_{anal.}$). It is clear that S_λ differs for each successive RI where the maximum value is 39310 (nm/RIU) while the minimum value was 2050 (nm/RIU). In general, S_λ increases with increasing RI but at particular value, S_λ deviate to be highest as mentioned above. The highest S_λ at RI (= 1.41) gives indication that the proposed sensor has capability to detect analytes with RIs differences of 0.001. Concerning on λ_{peak}, it shits towards the longer wavelength with increasing RIs while α_{loss} increases moderately and increases rapidly when RI (=1.42). Table 2 exhibits the performance of sensor via the parameters that have calculated by assisting **Fig. 4 when** RI varies from 1.38 to 1.42

Table 2. Performance of sensor when RI varies from 1.38 to 1.42

n_{ana}	λ_{peak} (nm)	Peak loss (dB/cm)	FWHM (nm)	S_S (nm/RIU)	R (RIU)	FOM 1/RIU
1.38	563.6	5.61	61.9	2050	4.88×10^{-5}	365.4
1.39	583.1	9.47	40.3	2630	3.8×10^{-5}	65.3
1.40	611	18.1	41.4	4080	2.45×10^{-5}	255.4
1.41	650.9	42.12	25.2	39310	2.54×10^{-7}	1559.9
1.42	1041	83.95	125.5	----	------	----

Another critical parameter that known as sensor resolution (R) and figure of merit (FOM) that can be calculated according to the equations [28].

$$R(RIU) = ٦ \times \Delta\,\lambda_{min} \quad (7)$$

$$\mathrm{FOM}\ (\mathrm{RIU}^{-1}) = S_\lambda(\mathrm{nm/RIU})/\mathrm{FWHM(nm)} \quad (8)$$

The reciprocal of sensitivity at successive refractive indices is defined by (٦) while($\Delta\,\lambda_{min}$), refers to peak wavelength resolution of instrument (almost is set to be 0.1nm). The most values of R was in the order of 10^{-5}. At $RI\,(=1.42)$, R is 2.54×10^{-7}(RIU). However, R is inversely proportional with S_λ, so, the high value of S_λ attained for proposed sensor will achieve good resolution to the sensor and this is necessary for various sensing purpose. λ_{peak}, peak loss, $FWHM$, and FOM as a function of RLs of analyte showed in Fig.5 and 6. Concerning on Fig.5, it shows the resonance wavelength and peak loss increase with increasing RI; it is clear that the trending is exponential so, the quadratic fitting tool was suitable to do curve fitting for resonance wavelength and loss peak. It obvious that correlation coefficient will be acceptable. Fig.6 (left) shows that FWHM increases with increasing RI and the behavior with RI is not linear. The equation presented for fitted data is quadratic and its choice was suitable. Fig.6 (right) shows FOM as a function of RLs of analyte, it clear that the same behavior is presented but forFOM, the correlation coefficient is large signifying on good behavior of FOM function.

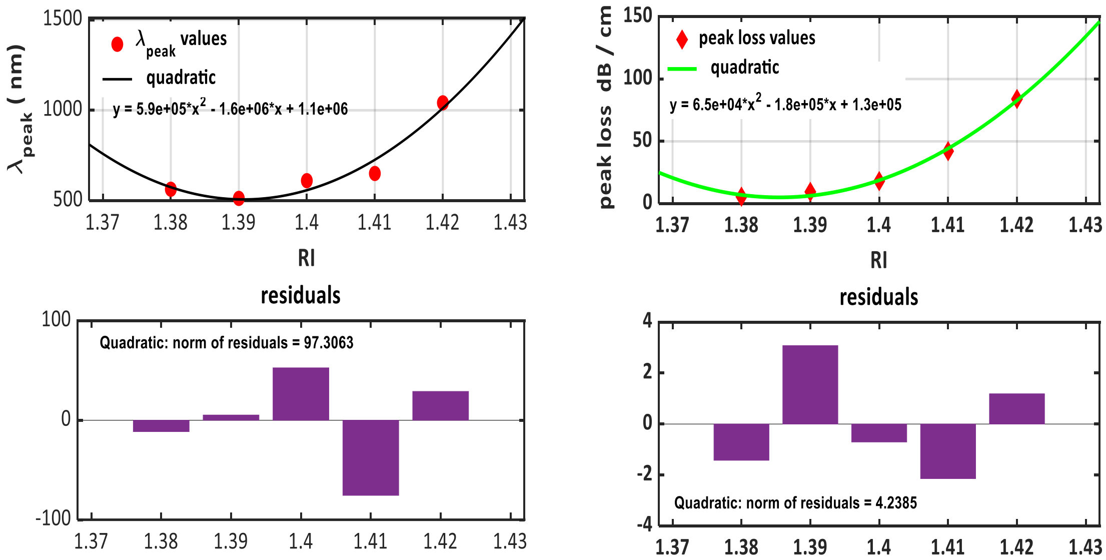

Fig. 5. λ_{peak} (left) and peak loss (right) against RIs of analytes.

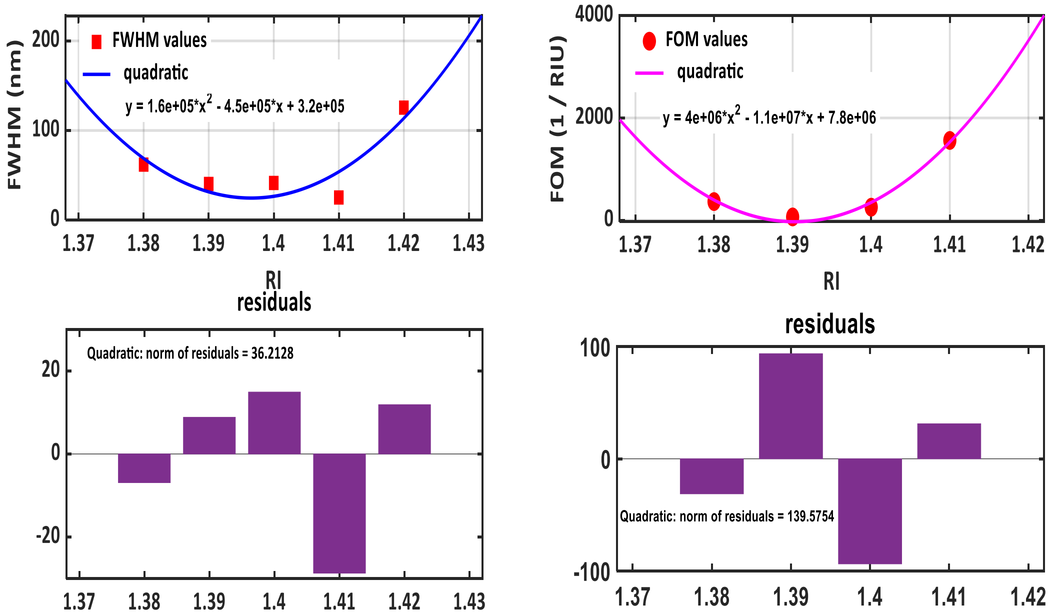

Fig. 6. FWHM (left) and peak FOM (right) against RI.

5. Conclusions

COMSOL Multiphysics software is used to design and analysis new Double Core Photonic Sensor Design Based on SPR that uses a faced layer of HfO2 for the sensing material to aid the plasmonic excitation to be taken place. The finding shows there is a high S_λ of 39310 (nm/RIU) and this value makes the proposed sensor has capability to detect analytes with RIs differences of 0.001 instead of 0.01 as presented in most publications. The minor differences that can be detected is between RIs from 1.38 to 1.42. Concerning on λ peak, peak loss, FWHM, and FOM as a function of RIs, the behaviour of these parameters was nonlinear and the correlation coefficient is different and is large FOM and peak loss.

6. References

[1] G. F. Andrade, M. Fan, and A. G. Brolo, "Multilayer silver nanoparticles-modified optical fiber tip for high performance SERS remote sensing," *Biosensors and Bioelectronics,* vol. 25, no. 10, pp. 2270-2275, 2010.

[2] B. Kuiri *et al.*, "Development of ring-core photonic crystal fiber based on LiNbO3 supporting higher-order OAM modes," *Optical and Quantum Electronics,* vol. 55, no. 8, p. 726, 2023.

[3] M. De, T. K. Gangopadhyay, and V. K. Singh, "Prospects of photonic crystal fiber as physical sensor: an overview," *Sensors,* vol. 19, no. 3, p. 464, 2019.

[4] B. Kuiri *et al.*, "Ultra-low loss polymer-based photonic crystal fiber supporting 242 OAM modes with high bending tolerance for multimode THz communication," *Results in Physics,* vol. 36, p. 105465, 2022.

[5] B. Kuiri *et al.*, "Design and optimization of photonic crystal fiber with low confinement loss guiding 98 OAM modes in THz band," *Optical Fiber Technology,* vol. 68, p. 102752, 2022.

[6] B. Kuiri, B. Dutta, N. Sarkar, S. Santra, R. Atta, and A. S. Patra, "Development of photonic crystal fiber supporting 124 OAM modes with flat dispersion and low confinement loss," *Optical and Quantum Electronics,* vol. 54, no. 8, p. 527, 2022.

[7] R. Q. M. B. M. Ahmed, "Optical Diagnostics of Zn foil using Non thermal plasma jets (NTPJ) via high voltage," *Mustansiriyah Journal of Pure and Applied Sciences,* vol. 2, no. 2, pp. 112-125, 2024.

[8] J. H. Osório, J. G. Hayashi, Y. A. Espinel, M. A. Franco, M. V. Andrés, and C. M. Cordeiro, "Photonic-crystal fiber-based pressure sensor for dual environment monitoring," *Applied Optics,* vol. 53, no. 17, pp. 3668-3672, 2014.

[9] Y. Wang, M. Yang, D. Wang, and C. Liao, "Selectively infiltrated photonic crystal fiber with ultrahigh temperature sensitivity," *IEEE Photonics Technology Letters,* vol. 23, no. 20, pp. 1520-1522, 2011.

[10] G. P. Agrawal, "Nonlinear fiber optics," in *Nonlinear Science at the Dawn of the 21st Century*: Springer, 2000, pp. 195-211.

[11] J. Lou, T. Cheng, S. Li, and X. Zhang, "Surface plasmon resonance photonic crystal fiber biosensor based on gold-graphene layers," *Optical Fiber Technology,* vol. 50, pp. 206-211, 2019.

[12] M. Abdullah-Al-Shafi and S. Sen, "Design and analysis of a chemical sensing octagonal photonic crystal fiber (O-PCF) based optical sensor with high relative sensitivity for terahertz (THz) regime," *Sensing and Bio-Sensing Research,* vol. 29, p. 100372, 2020.

[13] J. N. Dash and R. Jha, "Graphene-based birefringent photonic crystal fiber sensor using surface plasmon resonance," *IEEE Photonics Technology Letters,* vol. 26, no. 11, pp. 1092-1095, 2014.

[14] B. A. Z. Z. M. Abood and A. A. Khadayeir, "Measurement of Electron temperature (Te) and Electron density (ne) Cold Plasma Jets Optical Emission Spectroscopy (OES) Method," *Mustansiriyah Journal of Pure and Applied Sciences,* vol. 2, no. 2, pp. 126-133, 2024.

[15] S. Chakma, M. A. Khalek, B. K. Paul, K. Ahmed, M. R. Hasan, and A. N. Bahar, "Gold-coated photonic crystal fiber biosensor based on surface plasmon resonance: design and analysis," *Sensing and bio-sensing Research,* vol. 18, pp. 7-12, 2018.
[16] V. S. Chaudhary, D. Kumar, G. P. Mishra, S. Sharma, and S. Kumar, "Plasmonic biosensor with gold and titanium dioxide immobilized on photonic crystal fiber for blood composition detection," *IEEE Sensors Journal,* vol. 22, no. 9, pp. 8474-8481, 2022.
[17] S. Mittal, T. Sharma, and M. Tiwari, "Surface plasmon resonance based photonic crystal fiber biosensors: A review," *Materials Today: Proceedings,* vol. 43, pp. 3071-3074, 2021.
[18] V. S. Chaudhary, D. Kumar, and S. Kumar, "Gold-immobilized photonic crystal fiber-based SPR biosensor for detection of malaria disease in human body," *IEEE sensors journal,* vol. 21, no. 16, pp. 17800-17807, 2021.
[19] J. N. Jabir and N. A. Areebi, "High sensitively of double-core surface plasmon resonance biosensor based on photonic crystal fiber," *Optical and Quantum Electronics,* vol. 54, no. 10, p. 626, 2022.
[20] W. Liu *et al.*, "Ultra-sensitive hexagonal PCF-SPR sensor with a broad detection range," *Journal of Modern Optics,* vol. 67, no. 20, pp. 1545-1554, 2020.
[21] S. Akter, M. Z. Rahman, and S. Mahmud, "Highly sensitive open-channels based plasmonic biosensor in visible to near-infrared wavelength," *Results in Physics,* vol. 13, p. 102328, 2019.
[22] Z. Salehnezhad, M. Soroosh, and A. Farmani, "Design and numerical simulation of a sensitive plasmonic-based nanosensor utilizing MoS2 monolayer and graphene," *Diamond and Related Materials,* vol. 131, p. 109594, 2023.
[23] A. Ehyaee, A. Rahmati, A. Bosaghzadeh, and S. Olyaee, "Machine learning-enhanced surface plasmon resonance based photonic crystal fiber sensor," *Optics Express,* vol. 32, no. 8, pp. 13369-13383, 2024.
[24] E. Silaeva, L. Saddier, and J.-P. Colombier, "Drude-lorentz model for optical properties of photoexcited transition metals under electron-phonon nonequilibrium," *Applied Sciences,* vol. 11, no. 21, p. 9902, 2021.
[25] M. Al-Kuhaili, "Optical properties of hafnium oxide thin films and their application in energy-efficient windows," *Optical Materials,* vol. 27, no. 3, pp. 383-387, 2004.
[26] W. Li, Y. Chen, J. Xu, M. Jiang, and H. Zou, "A D-shaped SPR-based PCF sensor with an extremely high-amplitude sensitivity for measuring the refractive index," *Micromachines,* vol. 14, no. 7, p. 1295, 2023.
[27] M. J. B. M. Leon and M. A. Kabir, "Design of a liquid sensing photonic crystal fiber with high sensitivity, bireferingence & low confinement loss," *Sensing and Bio-Sensing Research,* vol. 28, p. 100335, 2020.
[28] N. S. Rahim and S. S. Al-Bassam, "Photonic crystal fiber Fabry–Perot interferometer for humidity sensor," *Journal of Optics,* vol. 53, no. 4, pp. 2937-2942, 2024.